RSC Advances

PAPER

View Article Online
View Journal | View Issue

Cite this: *RSC Adv.*, 2020, **10**, 31547

Facile synthesis of picenes incorporating imide moieties at both edges of the molecule and their application to *n*-channel field-effect transistors†

Yuxin Guo,[a] Kaito Yoshioka,[a] Shino Hamao,[b] Yoshihiro Kubozono,[*b] Fumito Tani,[c] Kenta Goto[c] and Hideki Okamoto[*a]

Received 10th June 2020
Accepted 17th August 2020

DOI: 10.1039/d0ra06629j

rsc.li/rsc-advances

Picene derivatives incorporating imide moieties along the long-axis direction of the picene core (C_n-PicDIs) were conveniently synthesized through a four-step synthesis. Photochemical cyclization of dinaphthylethenes was used as the key step for constructing the picene skeleton. Field-effect transistor (FET) devices of C_n-PicDIs were fabricated by using ZrO_2 as a gate substrate and their FET characteristics were investigated. The FET devices showed normally-off *n*-channel operation; the averaged electron mobility (μ) was evaluated to be 2(1) $\times$ 10^{-4}, 1.0(6) $\times$ 10^{-1} and 1.4(3) $\times$ 10^{-2} cm^2 V^{-1} s^{-1} for C_4-PicDI, C_8-PicDI and C_{12}-PicDI, respectively. The maximum μ value as high as 2.0 $\times$ 10^{-1} cm^2 V^{-1} s^{-1} was observed for C_8-PicDI. The electronic spectra of C_n-PicDIs in solution showed the same profiles irrespective of the alkyl chain lengths. In contrast, in thin films, the UV absorption and photoelectron yield spectroscopy (PYS) indicated that the lowest unoccupied molecular orbital (LUMO) level of C_n-PicDIs gradually lowered upon the elongation of the alkyl chains, suggesting that the alkyl chains modify intermolecular interactions between the C_n-PicDI molecules in thin films. The present results provide a new strategy for constructing a high performance *n*-channel organic semiconductor material by utilizing the electronic features of phenacenes.

1 Introduction

Development of organic semiconductors, that enables the fabrication of high performance electronic devices, namely, organic field-effect transistors (FETs), is critical for the production of electronics in the near future.[1] By replacing the conventional silicon-based semiconductors with organic materials, the energy and cost of fabricating electronic devices can be reduced, and light-weight and flexible devices will be attained. For the realization of full-organic electronics, hole-transporting (*p*-channel) and electron-transporting (*n*-channel) materials are desired because such materials provide complementary metal-oxide-semiconductor (CMOS) logic circuits[2,3] and organic/polymer photovoltaics.[4–6]

In the last two decades, a huge number of *p*-channel organic small-molecule FETs were studied from the aspects of both preparing suitable materials and device fabrication techniques.[7–9] Thus, organic molecules achieving a hole mobility exceeding 10 cm^2 V^{-1} cm^{-1} have been reported, *e.g.*, [1]benzothieno[3,2-*b*][1]benzothiophene (BTBT)[10] and related thiophene-fused polycyclic aromatics.[11–15] The present authors have investigated phenacene-based organic FETs to demonstrate that phenacenes are promising *p*-type semiconductors.[16,17] Namely, single-crystal FETs of [9]phenacene and thin-film FETs of 3,10-ditetradecylpicene ($(C_{14}H_{29})_2$-picene) displayed carrier mobility (μ) as high as 18 and 21 cm^2 V^{-1} cm^{-1}, respectively.[18,19] Additionally, they have demonstrated that complementary logic circuits, such as a flexible CMOS inverter by using phenacenes as *p*-channel materials, were realized.[20,21]

In contrast to the successful developments and applications of *p*-channel materials, those of high-performance *n*-channel organic semiconductors are still a challenging task because appropriate molecular design is necessary to stabilize both the molecule and radical anion under the device operation conditions. Conventionally, *n*-channel materials were designed by introducing strongly electron-withdrawing moieties into π-extended aromatic molecules.[22,23] 3,4:9,10-Perylenetetracarboxylic diimides (**PTCDIs**) and naphthalene-1,8:4,5-tetracarboxylic diimides (**NDIs**) are representative *n*-channel organic semiconductors and their chemical modifications are being continued to obtain air-stable and high-mobility materials.[24–26]

[a]*Division of Earth, Life, and Molecular Sciences, Graduate School of Natural Science and Technology, Okayama University, Okayama 700-8530, Japan. E-mail: hokamto@okayama-u.ac.jp*

[b]*Research Institute for Interdisciplinary Science, Okayama University, Okayama 700-8530, Japan*

[c]*Institute for Materials Chemistry and Engineering, Kyushu University, Fukuoka 819-0395, Japan*

† Electronic supplementary information (ESI) available: Experimental details, FET parameters of C_n-PicDIs, NMR spectra of new compounds, theoretical calculation results. See DOI: 10.1039/d0ra06629j

Heteroacenes are an another approach to *n*-channel material, thus, tetraazapentacene derivatives were reported to display electron mobility as high as 27.8 $cm^2\ V^{-1}\ cm^{-1}$.[27] Also, for benzodifurandione-oligo-(*p*-phenylenevinylene) (BDOPV) derivatives, the highest electron mobility exceeding 10 $cm^2\ V^{-1}\ s^{-1}$ was recorded.[28]

Phenacenes are quite stable polycyclic aromatic hydrocarbons. Large phenacenes, having imide moieties in the branching directions along the long molecular axis and the related polycyclic aromatic diimides were previously synthesized.[29–31] Wang *et al.* reported that the diimide derivatives of dibenzo[*a*,*h*]anthracene and phenanthro[1,2-*b*]chrysene served as active layers of *n*-channel FET devices displaying electron mobility up to 0.054 $cm^2\ V^{-1}\ cm^{-1}$.[29] However, few literature on *n*-channel FET application of phenacene diimides is available. Furthermore, little information either on synthesis of phenacene derivatives incorporating imide moieties in the long-axis directions of the molecules or on their *n*-channel semiconductor application has so far been available.

Therefore, it would be of interest to construct an *n*-channel material based on the unique electronic frameworks of phenacene and evaluate the FET properties to develop a new *n*-channel organic semiconductor. In the present study, we prepared picene derivatives, **C_n-PicDI**s (n = 4, 8 and 12, see Fig. 1 for the chemical structures), as the first imide-incorporating picenes at the both edges of the molecule and evaluated their *n*-channel FET characteristics.

2 Results and discussion

2.1 Synthesis of C_n-PicDIs

The synthetic route to **C_n-PicDI**s is shown in Scheme 1. The structures of the new compounds were determined by NMR and IR spectra as well as elemental analysis or high-resolution mass spectrometry. The full characterization data and the NMR spectra are deposited in ESI.† Conventionally, phenacene frameworks have been constructed by the Mallory photoreaction.[32] Because the photochemical strategy is one of the most convenient and reliable pathways toward phenacene frameworks, we used the photoreaction in the final step.

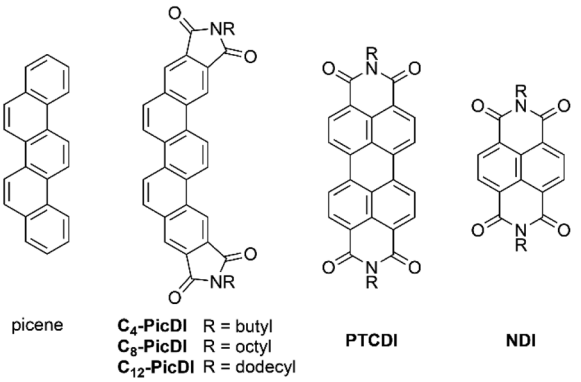

Fig. 1 Chemical structures of parent picene, C_n-PicDIs and related aromatic diimides (PTCDI, NDI).

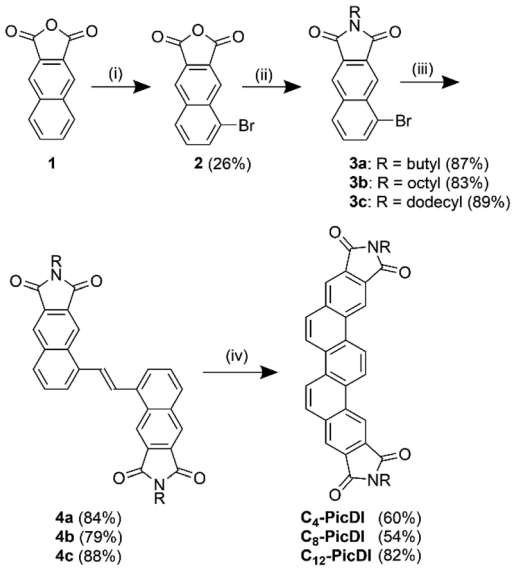

Scheme 1 Synthetic route to C_n-PicDIs. Reagents and conditions: (i) Br_2, NaOH, H_2O. (ii) RNH_2, AcOH. (iii) (*E*)-$Bu_3SnCH{=}CHSnBu_3$, $Pd(PPh_3)_4$, toluene. (iv) $h\nu$ (352 nm), I_2, air, CH_2Cl_2.

Bromo-substituted naphthalimides **3a–c** were obtained in two steps from commercially available 2,3-naphthalenedicarboxylic anhydride **1**. Bromonaphthalimides **3** were efficiently converted to diarylethenes **4** through a Stille coupling reaction with (*E*)-1,2-bis(tributylstannyl)ethene using $Pd(PPh_3)_4$ as a catalyst. Diarylethenes **4a–c** were then subjected to Mallory photoreaction, thus, they were irradiated with black-light lamps (352 nm, 6 × 15 W) in the presence of 10 mol% of I_2 to afford desired **C_n-PicDI**s in moderate to good yields. In the photoreaction, the (*E*)-form of **4** photochemically isomerized to the corresponding (*Z*)-form which subsequently cyclized to afford **C_n-PicDI**s.

2.2 Electronic spectra in solution and crystalline states

Fig. 2 shows UV-vis and fluorescence emission spectra of **C_n-PicDI**s in $CHCl_3$ with those of parent picene as the reference. Parent picene showed absorption bands at λ_{max}^{Abs} 376 nm with small intensity and at 329 nm with moderate intensity. Fluorescence band of picene was observed at λ_{max}^{FL} 378 nm with clear vibrational structure. **C_n-PicDI**s displayed absorption bands at

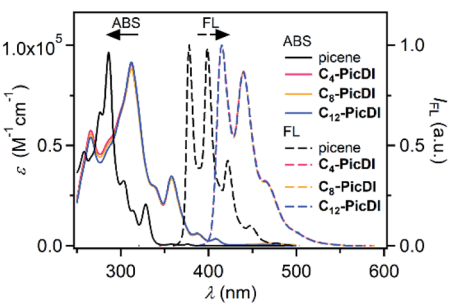

Fig. 2 Absorption and fluorescence spectra of C_n-PicDIs and parent picene in $CHCl_3$.

λ_{max}^{Abs} 408 and 358 nm and fluorescence one at λ_{max}^{FL} 415 nm irrespective of the alkyl chain length at the imide moieties. Therefore, the alkyl chain length little affected the electronic features of **C_n-PicDI**s in solution. The absorption and fluorescence spectra of **C_n-PicDI**s red-sifted by 30 nm and 37 nm, respectively, compared to those of parent picene. These results suggest effective conjugation between the picene π system and the two imide moieties. Additionally, the spectral red-shift could be due to contribution from intramolecular charge transfer between the picene core and the imide moieties. As seen from Fig. 3, HOMO of **C_n-PicDI**s locates on the central picene moiety while LUMO extends over the entire molecule including the imide moieties.

Fluorescence emission spectra of **C_n-PicDI**s were measured in the crystalline state to obtain an insight into their solid state electronic features (Fig. S1 of ESI†). **C_4-PicDI** showed a broad emission band with a maximum at λ_{max}^{FL} 486 nm. **C_{12}-PicDI** showed an emission profile (λ_{max}^{FL} 473 nm) similar to that of **C_4-PicDI**. In the case of **C_8-PicDI** the emission wavelength region was the same as that of **C_4**- and **C_{12}-PicDI**s, however, the profile of the emission band was different from that of **C_4**- and **C_{12}-PicDI**s. These results may indicate that intramolecular interactions were affected by the alkyl chain length of the imide part in the solid state. Unfortunately, single crystals of **C_n-PicDI**s suitable for X-ray crystallographic analysis were not obtained, we are currently unable to discuss details on the specific intermolecular interactions in solid state.

2.3 Theoretical analysis for the electronic features

Theoretical calculations were performed to investigate electronic features of **C_n-PicDI**s. The molecular geometries of **C_n-PicDI**s were optimized by density functional theory (DFT) at the B3LYP/6-31+G(d) level of theory and the optimized atomic coordinates are deposited in Tables S3–S6 of ESI.† Also, the optimized molecular structure of **C_8-PicDI** was shown in Fig. S4 of ESI† as the representative result. The picenediimide core was calculated to be in a flat geometry.

Fig. 3 shows molecular orbital (MO) diagrams of **C_8-PicDI** and parent picene. The LUMO energy levels of **C_8-PicDI** (−2.75 eV) was much lower than that of picene (−1.59 eV) suggesting that the charge-transporting state was stabilized by the strongly electron withdrawing imide moieties. The imide moieties effectively interact with the electronic core of picene in **C_8-PicDI** to modify the molecular orbital levels. As a result, the LUMO and LUMO+1 levels are inverted between parent picene and **C_8-PicDI**. **C_4-PicDI** and **C_{12}-PicDI** showed the same electronic features as **C_8-PicDI**. The LUMO of **C_8-PicDI** has less nodal planes along the long axis of the molecule compared to the case of parent picene. It is, thus, expected that such an electronic nature facilitates efficient overlapping of the molecular orbitals resulting in strong interactions between **C_n-PicDI** molecules in the charge-transporting state in solid state.[13]

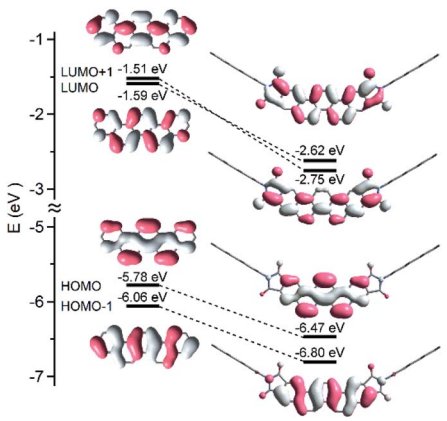

Fig. 3 Molecular orbital diagrams for picene (left) and C_8-PicDI (right) calculated at the B3LYP/6-31+G(d) level.

2.4 Structures and electronic properties in thin films

Fig. 4(a) shows X-ray diffraction (XRD) patterns of thin films of **C_n-PicDI**s exhibiting only 00*l* Bragg reflections; the process of fabrication of the thin films is the same as that for the thin films for FET devices (see ESI†). The $1/|c^*|$ values were determined to be 22.94(7) Å, 31.0(1) Å and 37.1(6) Å, respectively, for $n = 4$, 8 and 12; c^* refers to the reciprocal lattice of lattice constant, c. The increase in $1/|c^*|$ against n is reasonable because the long-axis length of **C_n-PicDI**s extends with n, *i.e.*, the long axis of **C_n-PicDI** molecules stands with almost normal to the substrate. Actually, as seen from Fig. 4(b), the long axis of **C_n-PicDI**s ($n = 4$, 8 and 12) are inclined by 30°, 29° and 32°, respectively, with respect to c^* axis. This inclined angle (θ) is almost the same as that, *ca.* 30°, of $(C_{14}H_{29})_2$-picene.[19]

As seen from Fig. 4(c), the electronic absorption spectra of thin films of **C_n-PicDI**s show that the onset energy changes slightly from 2.87 eV to 2.92 eV with an increase in n, indicating that the HOMO–LUMO gap does not vary significantly with extended alkyl chains. On the other hand, the photoelectron yield spectroscopy (PYS) (Fig. 4(d)) shows that the onset energy increases gradually from 6.63 eV to 6.91 eV with an increase in n. This implies that the HOMO level lowers with n.

Fig. 5 shows the energy levels of HOMO and LUMO determined experimentally for **C_n-PicDI**s in comparison to parent picene and *N*,*N*′-dioctyl-3,4:9,10-perylenedicarboximide (**PTCDI-C_8**, see Fig. 1 for structure, R = octyl) as the reference materials. The LUMO levels are located in an energy range of −3.76 eV to −3.99 eV, indicating that the LUMO level lies in the lower energy range than the LUMO levels (−2.2 eV to −2.9 eV) of parent phenacene molecules[33] which have provided good *p*-channel FET operation. The energy (−3.76 eV to −3.99 eV) for the LUMO levels of **C_n-PicDI**s suggests a potential *n*-channel FET operation.

It is important to reveal structure-mobility relationship to design a novel *n*-channel material. For **C_nPicDI**s, single crystals appropriate for X-ray crystallographic analysis were not obtained in this study. Detailed structural analysis for **C_n-PicDI**s in crystalline and thin films are underway.

2.5 *n*-Channel FET characteristics

Fig. 6(a) shows a device structure of **C_n-PicDI** thin-film FET with a ZrO_2 gate dielectric; the commercially available ZrO_2 thin film

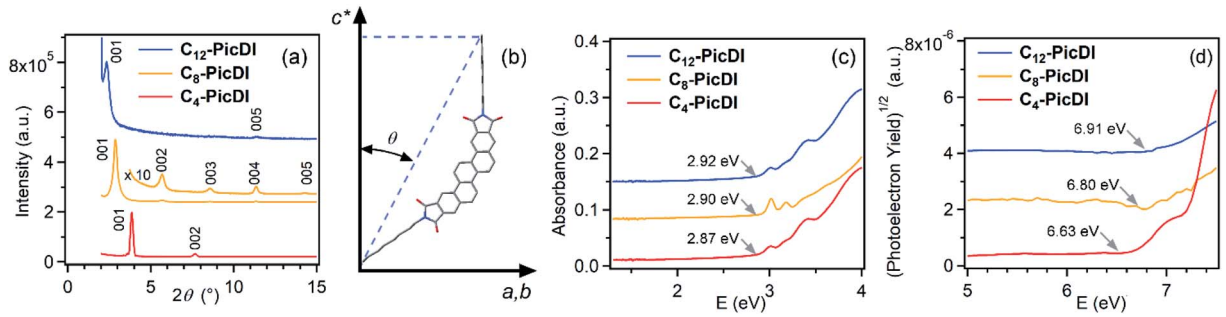

Fig. 4 (a) XRD patterns of thin films of C_n-PicDIs formed on an SiO_2 substrate. (b) Orientation of the long axis of the C_n-PicDI molecule with respect to c^* axis (normal to *ab* plane) in the thin film formed on an SiO_2 substrate. (c) Electronic absorption spectra of thin films of C_n-PicDIs formed on quartz glass. (d) PYS spectra of thin films of C_n-PicDIs formed on SiO_2/Si substrate.

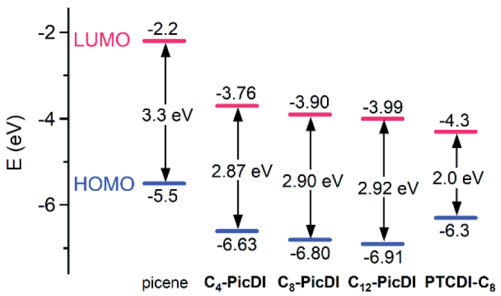

Fig. 5 Energy diagrams for HOMO and LUMO of picene, C_n-PicDIs, and PTCDI-C_8 experimentally determined by PYS and electronic absorption spectra in thin films. The data for picene and PTCDI-C_8 are taken from ref. 16 and 34, respectively.

prepared by RF sputtering was used in this study. The device structure corresponds to a typical top-contact bottom-gate type. Details of device fabrication procedure are described in experimental section of ESI.† A 3 nm thick 2,3,5,6-tetrafluorotetracyanoquinodimethane (F4TCNQ) layer was inserted to reduce contact resistance between the active layer and source (S)/drain (D) electrodes (Fig. 6(a)). Here, it should be stressed that F4TCNQ is not doped to the channel region but underneath the electrodes. Namely, only contact resistance is decreased by the F4TCNQ doping. The transfer and output characteristics of **C_8-PicDI** thin-film FET measured under an argon atmosphere are shown in Fig. 6(b) and (c), respectively, which show typical *n*-channel normally-off FET characteristics. Thus, as expected from the energy diagram shown in Fig. 5, a clear *n*-channel operation was obtained.

The FET parameters for seven **C_8-PicDI** thin-film FET devices are listed in Table 1. The values of averaged μ ($\langle\mu\rangle$) and V_{th} ($\langle V_{th}\rangle$) are $1.0(6) \times 10^{-1}$ cm^2 V^{-1} s^{-1} and 20(2) V, respectively. All measurements of FET properties were done in Ar atmosphere (see ESI†). The maximum field-effect mobility (μ) was determined to be 2.0×10^{-1} cm^2 V^{-1} s^{-1} from the transfer curve (Fig. 6(b)) in the saturation regime with normal formula.[35] The above μ value is relatively high in *n*-channel organic thin-film

Table 1 FET parameters of **C_8-PicDI** thin-film FET with ZrO_2 gate dielectric[a]

Sample	μ (cm^2 V^{-1} s^{-1})	V_{TH} (V)	on/off	S (V per decade)
#1	0.64×10^{-1}	18.8	2.0×10^4	1.87
#2	1.4×10^{-1}	17.2	6.4×10^4	1.08
#3	0.95×10^{-1}	17.5	3.7×10^4	1.24
#4	0.22×10^{-1}	20.0	1.0×10^4	1.78
#5	2.0×10^{-1}	20.4	2.6×10^4	0.890
#6	0.98×10^{-1}	21.5	1.5×10^4	1.05
#7	1.0×10^{-1}	21.5	1.7×10^4	1.00
Average	$1.0(6) \times 10^{-1}$	20(2)	$3(2) \times 10^4$	1.3(4)

[a] The parameters were determined from the forward transfer curves.

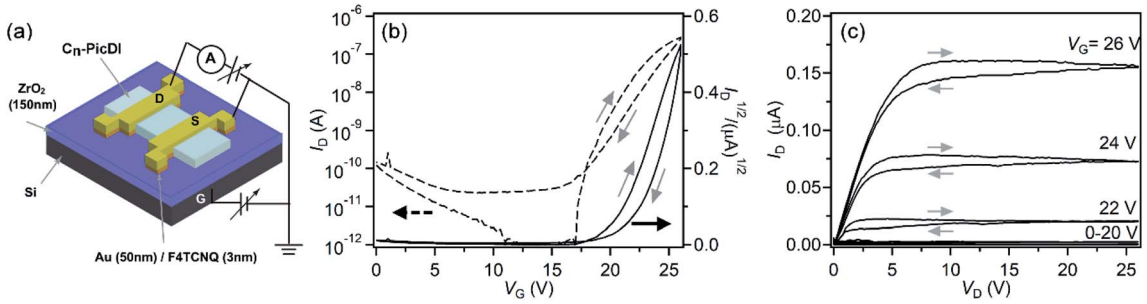

Fig. 6 (a) Device structure of C_n-PicDI FETs. (b) Transfer and (c) output curves of C_8-PicDI thin-film FETs with ZrO_2 gate dielectric. This FET refers to device #5 in Table 1.

FETs, *i.e.*, the value is almost the same as that in **PTCDI-C$_8$** thin-film FET which is normally employed for *n*-channel FET.[24–26] Also the relatively low voltage operation (V_{th} = 20.4 V) is achieved in **C$_8$-PicDI** thin-film FET because of the usage of high-*k* gate dielectric (ZrO_2), but the V_{th} value is a little higher in comparison with that ($V_{th} \sim 2.9$ V) of **PTCDI-C$_8$** thin film FET using ZrO_2 gate dielectric (evaluated in this study, data not shown). This is due to higher LUMO level of **C$_n$-PicDI**s than that of **PTCDI-C$_8$** as seen from Fig. 4. Herein, we comment a little large hysteresis observed in transfer and output curves (Fig. 6(b) and (c)). The hysteresis may be due to the bias stress effect, which is observed in non-hydrophobic surface of gate dielectric. Therefore, a parylene-coating of ZrO_2 employed in this study may not provide a sufficient hydrophobic surface. This must be further ameliorated.

The FET characteristics of **C$_4$-PicDI** and **C$_{12}$-PicDI** thin-film FETs with ZrO_2 gate dielectric also showed *n*-channel normally-off FET properties (see Fig. S2 and S3 of ESI† for the transfer and output curves). Tables S1 and S2 of ESI† list the FET parameters of four **C$_4$-PicDI** thin-film FETs and eight **C$_{12}$-PicDI** thin-film FETs, respectively. The highest μ values for **C$_4$-PicDI** and **C$_{12}$-PicDI** thin-film FETs were 2.7×10^{-4} cm^2 V^{-1} s^{-1} and 1.9×10^{-2} cm^2 V^{-1} s^{-1}, respectively. Thus, the μ value for **C$_4$-PicDI** thin-film FET was two-three orders of magnitude lower than that for **C$_8$-PicDI** and **C$_{12}$-PicDI**. At the present stage, **C$_8$-PicDI** provides the highest μ value among the **C$_n$-PicDI**s investigated. The reason is still unclear, but the higher energy level of LUMO (−3.76 eV) might provide the poorer FET properties of **C$_4$-PicDI**. In addition, the difference in μ between **C$_8$-PicDI** and **C$_{12}$-PicDI** may not be due to the energy levels of LUMO (−3.90 eV for **C$_8$-PicDI** and −3.99 eV for **C$_{12}$-PicDI**) but the crystallinity of thin films *i.e.*, poorer crystallinity in **C$_{12}$-PicDI** thin film as seen from the XRD patterns (Fig. 4(a)). As a consequence, the best material for *n*-channel FET operation is **C$_8$-PicDI** among the **C$_n$-PicDI** molecules. Such suitable alkyl chains for active layers of FET devices are reported for various organic semiconductor compounds.[10,36] Admittedly, **C$_8$-PicDI** would be a promising material for *n*-channel FET operation owing to the high μ value as high as 2.0×10^{-1} cm^2 V^{-1} s^{-1}. In addition, the FET properties were not recorded in ambient atmosphere, but it would be very important because *n*-channel operation drastically degrades under air. This would be a future significant work.

Finally, we briefly comment FET properties of **C$_n$-PicDI** thin-film FETs with an SiO_2 gate dielectric. *n*-Channel properties were found for the **C$_4$-PicDI** and **C$_8$-PicDI** thin-film FETs by applying higher voltage than 90 V, but the observed I_d value was lower than 10^{-9} A above 120 V; the V_{th} values were 110 V for **C$_4$-PicDI** and 98 V for **C$_8$-PicDI**. The results indicate that high-*k* gate dielectric is required for stable *n*-channel operation in **C$_n$-PicDI** thin-film FETs. From these points, the V_{th} value of 20(2) V in **C$_8$-PicDI** thin-film FET with ZrO_2 gate dielectric may be prominent.

3 Conclusions

Picene derivatives bearing imide moieties at the both edges of the molecule (**C$_n$-PicDI**s) were successfully synthesized by using the Mallory photoreaction as the key step. **C$_n$-PicDI**s are, to the best of our knowledge, the first phenacene derivatives possessing imide moieties in the long-axis direction of the framework. It was revealed that **C$_n$-PicDI**s served as the active layer of *n*-channel FET devices with high electron mobility. The highest μ value recorded for **C$_8$-PicDI** (2.0×10^{-1} cm^2 V^{-1} s^{-1}) was comparable to μ values of **PTCDI**s which were benchmark molecules of *n*-channel FET materials. Moreover, we point out that the usage of Ag metal for source/drain electrodes may lead to the higher value of μ owing to the reduction of carrier injection barrier height. This would be a future task. The present results would contribute to molecular design of new *n*-channel organic semiconductors which are highly desired in the current organic electronics.

Conflicts of interest

There are no conflicts to declare.

Acknowledgements

The present study was partly supported by Grants-in-Aid for Scientific Research, KAKENHI, from MEXT (26105004, 17K05976, 17K05500, 18K04940, 18K18736, 19H02676 and 20K05648) and by the Cooperative Research Program of the 'Network Joint Research Center for Materials and Devices' from MEXT, Japan. This work was the result of using research equipment shared in MEXT Project for promoting public utilization of advanced research infrastructure (program for supporting introduction of the new sharing system) Grant Number JPMXS0422300120.

Notes and references

1 S. R. Forrest, *Nature*, 2004, **428**, 911–918.
2 G. Schweicher, G. Garbay, R. Jouclas, F. Vibert, F. Devaux and Y. H. Geerts, *Adv. Mater.*, 2020, 1905909.
3 Y. Xu, C. Liu, D. Khim and Y.-Y. Noh, *Phys. Chem. Chem. Phys.*, 2015, **17**, 26553–26574.
4 J. Yang, B. Xiao, A. Tang, J. Li, X. Wang and E. Zhou, *Adv. Mater.*, 2019, **31**, 1804699.
5 C. Zhao, J. Wang, J. Jiao, L. Huang and J. Tang, *J. Mater. Chem. C*, 2020, **8**, 28–43.
6 C. Lee, S. Lee, G.-U. Kim, W. Lee and B. J. Kim, *Chem. Rev.*, 2019, **119**, 8028–8086.
7 C. Wang, H. Dong, L. Jiang and W. Hu, *Chem. Soc. Rev.*, 2018, **47**, 422–500.
8 J. Mei, Y. Diao, A. L. Appleton, L. Fang and Z. Bao, *J. Am. Chem. Soc.*, 2013, **135**, 6724–6746.
9 Y. Yuan, G. Giri, A. L. Ayzner, A. P. Zoombelt, S. C. B. Mannsfeld, J. Chen, D. Nordlund, M. F. Toney, J. Huang and Z. Bao, *Nat. Commun.*, 2014, **5**, 3005.
10 K. Takimiya, I. Osaka, T. Mori and M. Nakano, *Acc. Chem. Res.*, 2014, **47**, 1493–1502.
11 H. Iino, T. Usui and J. Hanna, *Nat. Commun.*, 2015, **6**, 6828.
12 K. Nakayama, Y. Hirose, J. Soeda, M. Yoshizumi, T. Uemura, M. Uno, W. Li, M. J. Kang, M. Yamagishi, Y. Okada,

E. Miyazaki, Y. Nakazawa, A. Nakao, K. Takimiya and J. Takeya, *Adv. Mater.*, 2011, **23**, 1626–1629.
13 C. Mitsui, T. Okamoto, M. Yamagishi, J. Tsurumi, K. Yoshimoto, K. Nakahara, J. Soeda, Y. Hirose, H. Sato, A. Yamano, T. Uemura and J. Takeya, *Adv. Mater.*, 2014, **26**, 4546–4551.
14 A. Yamamoto, Y. Murata, C. Mitsui, H. Ishii, M. Yamagishi, M. Yano, H. Sato, A. Yamano, J. Takeya and T. Okamoto, *Adv. Sci.*, 2018, **5**, 1700317.
15 T. Okamoto, C. P. Yu, C. Mitsui, M. Yamagishi, H. Ishii and J. Takeya, *J. Am. Chem. Soc.*, 2020, **142**, 9083–9096.
16 H. Okamoto, N. Kawasaki, Y. Kaji, Y. Kubozono, A. Fujiwara and M. Yamaj, *J. Am. Chem. Soc.*, 2008, **130**, 10470–10471.
17 Y. Kubozono, X. He, S. Hamao, K. Teranishi, H. Goto, R. Eguchi, T. Kambe, S. Gohda and Y. Nishihara, *Eur. J. Inorg. Chem.*, 2014, 3806–3819.
18 Y. Shimo, T. Mikami, S. Hamao, H. Goto, H. Okamoto, R. Eguchi, S. Gohda, Y. Hayashi and Y. Kubozono, *Sci. Rep.*, 2016, **6**, 21008.
19 H. Okamoto, S. Hamao, H. Goto, Y. Sakai, M. Izumi, S. Gohda, Y. Kubozono and R. Eguchi, *Sci. Rep.*, 2014, **4**, 5048.
20 E. Pompei, C. Turchetti, S. Hamao, A. Miura, H. Goto, H. Okamoto, A. Fujiwara, R. Eguchi and Y. Kubozono, *J. Mater. Chem. C*, 2019, **7**, 6022–6033.
21 Y. Shimo, T. Mikami, H. T. Murakami, S. Hamao, H. Goto, H. Okamoto, S. Gohda, K. Sato, A. Cassinese, Y. Hayashi and Y. Kubozono, *J. Mater. Chem. C*, 2015, **3**, 7370–7378.
22 Y. Sakamoto, T. Suzuki, M. Kobayashi, Y. Gao, Y. Fukai, Y. Inoue, F. Sato and S. Tokito, *J. Am. Chem. Soc.*, 2004, **126**, 8138–8140.
23 M. A. Kobaisi, S. V. Bhosale, K. Latham, A. M. Raynor and S. V. Bhosale, *Chem. Rev.*, 2016, **116**, 11685–11796.
24 X. Zhan, A. Facchetti, S. Barlow, T. J. Marks, M. A. Ratner, M. R. Wasielewski and S. R. Marder, *Adv. Mater.*, 2011, **23**, 268–284.
25 M. Gsänger, D. Bialas, L. Huang, M. Stolte and F. Würthner, *Adv. Mater.*, 2016, **28**, 3615–3645.
26 F. Würthner and M. Stolte, *Chem. Commun.*, 2011, **47**, 5109–5115.
27 M. Chu, J.-X. Fan, S. Yang, D. Liu, C. F. Ng, H. Dong, A.-M. Ren and Q. Miao, *Adv. Mater.*, 2018, **30**, 1803467.
28 J.-H. Dou, Y.-Q. Zheng, Z.-F. Yao, Z.-A. Yu, T. Lei, X. Shen, X.-Y. Luo, J. Sun, S.-D. Zhang, Y.-F. Ding, G. Han, Y. Yi, J.-Y. Wang and J. Pei, *J. Am. Chem. Soc.*, 2015, **137**, 15947–15956.
29 R. Wang, K. Shi, K. Cai, Y. Guo, X. Yang, J.-Y. Wang, J. Pei and D. Zhao, *New J. Chem.*, 2016, **40**, 113–121.
30 T. S. Moreira, M. Ferreira, A. Dall'armellina, R. Cristiano, H. Gallardo, E. A. Hillard, H. Bock and F. Durola, *Eur. J. Org. Chem.*, 2017, 4548–4551.
31 G. Naulet, S. Huet-Exiga, H. Bock and F. Durola, *Org. Chem. Front.*, 2019, **6**, 994.
32 F. B. Mallory and C. W. Mallory, *Org. React.*, 1984, **30**, 1–456.
33 H. Okamoto, S. Hamao, R. Eguchi, H. Goto, Y. Takabayashi, Y.-H. Yen, L. U. Liang, C.-W. Chou, G. Hoffmann, S. Gohda, H. Sugino, Y. Liao, H. Ishii and Y. Kubozono, *Sci. Rep.*, 2019, **9**, 4009.
34 N. Hiroshiba, R. Hayakawa, T. Chikyow, Y. Yamashita, H. Yoshikawa, K. Kobayashi, K. Morimoto, K. Matsuishi and Y. Wakayama, *Phys. Chem. Chem. Phys.*, 2011, **13**, 6280–6285.
35 S. M. Sze, *Semiconductor Devices: Physics and Technology*, 2nd ed., John Willey & Sons, Inc., UK, 2001.
36 H. Inokuchi, G. Saito, P. Wu, K. Seki, T. B. Tang, T. Mori, K. Imaeda, T. Enoki, Y. Higuchi, K. Inaka and N. Yasuoka, *Chem. Lett.*, 1986, **15**, 1263–1266.